# Rotationally resolved zero-kinetic-energy photoelectron spectrum of nitrogen

F. Merkt
*Department of Chemistry, Lensfield Road, Cambridge CB2 1EW, United Kingdom*

T. P. Softley
*Physical Chemistry Laboratory, South Parks Road, Oxford OX1 3QZ, United Kingdom*
(Received 27 January 1992)

Rotationally resolved zero-kinetic-energy (ZEKE) photoelectron spectra of the $X\,^2\Sigma_g^+(v^+=0,1) \leftarrow X\,^1\Sigma_g^+(v=0)$ bands of nitrogen have been recorded. The spectra show unexpected rotational-line intensities. The intensity distortions are explained by channel interactions. The strong $S$ and $U$ branches [$(N^+-J'')=+2$ and $+4$, respectively] of the (1-0) band borrow intensity from a nearly degenerate Rydberg state, converging to an electronic excited state of the ion, by a complex resonance mechanism. Field-induced rotational autoionization is shown to enhance the $O$ branch and $M$ branch [$(N^+-J'')=-2$ and $-4$] intensity of the (0-0) band. Recording ZEKE spectra with extraction fields of 10–100 V/cm appears to be an attractive and powerful way of obtaining spectroscopic information on Rydberg states with simultaneously high principal quantum number $n$ and high total-angular-momentum quantum number $J$.

PACS number(s): 33.20.Ni, 33.80.Eh

## I. INTRODUCTION

The development of zero-kinetic-energy photoelectron spectroscopy (ZEKEPES) has led to the obtaining of full rotational resolution in the photoelectron spectra of several small molecules. (For a recent review of the history of the technique, see Ref. [1].) The technique is based on ionization of high Rydberg states lying within a few $cm^{-1}$ of the ionization threshold by a weak electric field (typically $\leq 2$ V/cm). As a consequence of the considerable improvement of the resolution that can be achieved in PES using that technique, interest has been regained in understanding the factors that govern rotational line intensities and selection rules in ZEKEPES. The purpose of this paper is to report the ZEKE photoelectron spectrum of $N_2$ and to discuss some anomalous intensity patterns observed in its resolved rotational structure.

The first theoretical model concerned with rotational line intensities in PES was developed by Buckingham, Orr, and Sichel [2] before the first rotationally resolved photoelectron spectrum was reported by Åsbrink [3]. It was extended by Itikawa [4] to take vibronic interactions into account. More recent work involved the simulation of ZEKE spectra by use of a full quantum-mechanical treatment [5], the prediction of general selection rules for ionization of diatomic [6] and polyatomic molecules [7] and the investigation of the influence of Cooper minima on rotational ion distributions [8].

Early one-photon ZEKE spectra [9–11] have been interpreted in the framework of the model developed in Ref. [2]. In this model, electronic transition intensities are calculated between the molecular orbital (expanded in a one-center basis set) from which the electron is ejected and a continuum one-electron function. It failed to account for some intensity patterns observed in the published ZEKE spectra of $O_2$ [12], $H_2O$ [13], $H_2$ [14], and NO [15]. In addition, a recent overview of unpublished data points to the observation of intensity anomalies in HCl, OH, $Na_2$, VO, $N_2O$ and $NO_2$ [16]. In the case of $O_2$, some unexpectedly large intensities were shown to be due to a shape resonance [12]. Anomalous rotational line intensities in the ZEKE spectrum of $H_2O$ could be accounted for by a mechanism of energy redistribution between core rotation and the Rydberg electron mediated by the Rydberg-core dipole interaction [17] analogous to the mechanism discussed in Sec. IV A of this paper. A similar mechanism has been proposed for intensity anomalies in NO [15].

Being a threshold technique, ZEKEPES is subject to the same type of intensity distortions (compared to conventional PES) as those observed in threshold photoelectron spectroscopy (TPES) [18–20] due to the coupling of the ionization continuum with some discrete degenerate autoionizing states. Such couplings are well established in TPES, even though it has often been difficult, if at all possible, to identify the perturber states in detail. These couplings, which result in distorted PES line intensities, will be referred to in the following as final-state interactions or channel interactions.

Very recently, we showed how differences between the conventional and the ZEKE photoelectron spectra of $H_2$ could be accounted for by such final-state interactions [14]. Since the Rydberg series of $H_2$ have been studied extensively [21], it was possible to identify both the perturber states and the mechanisms leading to anomalous intensities in the ZEKE spectrum: Window resonances, complex resonances, and rotational autoionization were all shown to have a large impact on ZEKE rotational-line intensities [14].

Conventional photoelectron spectra involving ionization to the ground electronic state of $N_2^+$ have been

 ©1992 The American Physical Society

recorded by many authors [22–26]. Early studies were primarily concerned with Franck-Condon factors. More recent studies at higher resolution were aimed at obtaining information on rotational contours and relative branch intensities either by deconvolution of low resolution spectra [25] or by recording high resolution (25 $cm^{-1}$) conventional photoelectron spectra [26]. In the cases where the branch structure of the spectra could be partially resolved, it appeared that vibrational bands of the $N_2^+X\,^2\Sigma_g^+ \leftarrow N_2X\,^1\Sigma_g^+$ transition are dominated by strong transitions with $(N^+-J'')=0$ (referred to as $Q$-branch lines in the following) and weaker transitions with $(N^+-J'')=\pm 2$ (referred to as $S$ and $O$ branches in the following). Here $N^+$ stands for the rotational quantum number of the ion and $J''$ for the rotational quantum number of the neutral molecule. Also, the $S$ branch appeared to be slightly more intense than the $O$ branch in these PES studies.

The rotational line intensities we observe in the ZEKE spectrum of the (0-0) and the (1-0) vibrational bands of the $N_2^+X\,^2\Sigma_g^+ \leftarrow N_2X\,^1\Sigma_g^+$ electronic transition hardly show any correlation with these PES intensities. In the ZEKE spectrum of the (0-0) band the $O$ branch is about one order of magnitude more intense than the $S$ branch. The enhanced intensity of the $O$ branch can be unambiguously attributed to field-induced rotational autoionization. An interesting consequence of that finding is that one can use the ZEKE method with larger than usual extraction fields to record high-resolution rotational autoionization spectra of a restricted number of Rydberg states with simultaneously high principal quantum number $n$ and high angular-momentum quantum number $J$, as will be shown in Sec. IV A. From such spectra it is possible to establish propensity rules for rotational autoionization in the presence of an electric field.

The ZEKE spectrum of the (1-0) band possesses a strong $U$ branch [i.e., a branch with $(N^+-J'')=4$] in addition to the expected $O$, $Q$, and $S$ branches. Here again, the anomalous intensities can be accounted for qualitatively by final-state interactions. The intensity of the unexpectedly strong lines in the spectrum seems to be gained by a complex resonance mechanism.

The results presented here confirm the importance of final-state interactions in ZEKE spectra.

## II. EXPERIMENT

The details of the experimental setup have been described elsewhere [10]. Only the general principles and characteristics are outlined here. The tunable extreme ultraviolet (XUV) light used in these experiments is produced by sum-frequency mixing of two laser beams in a pulsed atomic beam of krypton. The wave number $\tilde{\nu}_1$ of the first laser beam is fixed at 47 046.8 $cm^{-1}$ so as to be in two-photon resonance with the $4p^5(^2P^0_{3/2})5p[\frac{1}{2}]$ $(J=0) \leftarrow 4p^6\,^1S$ transition in Kr, while the wave number $\tilde{\nu}_2$ of the second laser is scanned between 31 000 and 34 500 $cm^{-1}$, thus producing XUV wave numbers $2\tilde{\nu}_1+\tilde{\nu}_2$ between around 125 000 and 128 500 $cm^{-1}$. This XUV radiation is separated from the fundamentals $\tilde{\nu}_1$ and $\tilde{\nu}_2$ and from other wave numbers produced by four-wave mixing (e.g., $3\tilde{\nu}_1$, $3\tilde{\nu}_2$, $2\tilde{\nu}_1-\tilde{\nu}_2$, . . . ) by a vacuum monochromator and is refocused into a molecular beam of $N_2$ (research-grade purity, used without further purification) between two extraction plates with grids, one of which is located at the end of a 20-cm-long electron flight tube. The flow in the molecular beam is such that hardly any cooling takes place and extensive rotational progressions can be observed.

The repetition rate of the laser is 10 Hz and the pulse length approximately 10 ns. At the time of the light pulses, the only electric field present in the ionization region is a small stray field ( $\leq 100$ mV/cm in our experiments). The effects of this stray field are threefold: First, it lowers the ionization thresholds by about 1.8 $cm^{-1}$; second, it sweeps out of the ionization region all electrons released by direct ionization or stray-field ionization. Finally, it can induce some channel interaction between Rydberg states converging to different rotational levels of the ion as will be discussed in Sec. IV A. After an adjustable delay time (typically 0.5–1.0 $\mu$s) an electric field (1–20 V/cm) is applied between the extraction plates to field ionize high-Rydberg states lying a few $cm^{-1}$ below the field-free thresholds and to send them along the electron flight tube, at the end of which they are detected by an electron multiplier.

The field ionization range $\Delta\tilde{\nu}$ caused by an electric field $E$ is given in first approximation by Eq. (1):

$$\Delta\tilde{\nu}/cm^{-1}=6\sqrt{E/(V/cm)}\ . \tag{1}$$

Equation (1) has been verified in a number of studies involving different atoms and molecules [14,27–31]. In some of the experiments reported here a combination of two ionization-extraction pulsed electric fields has been used to improve the resolution as has been illustrated in Ref. [14]. The first discrimination field $E_1$ is applied immediately after the laser pulse, while the second, delayed field $E_2$ produces the detected electrons. In this case, the field ionization range is given by Eq. (2):

$$\Delta\tilde{\nu}/cm^{-1}=6[\sqrt{E_2/(V/cm)}-\sqrt{E_1/(V/cm)}]\ . \tag{2}$$

The main factors determining the resolution of the obtained ZEKE spectra are the following.

(i) The magnitude of the extraction field(s) determines the field ionization range (i.e., the frequency range below the field-free ionization threshold over which electrons are released) according to Eqs. (1) or (2).

(ii) Slowly rising extraction fields ionize highest-Rydberg states before ionizing lower-Rydberg states. By gating the electron signal it is possible to discriminate between electrons released at different times and hence achieve a resolution that is higher than predicted by Eqs. (1) or (2) [31] and, in the end, comparable with our XUV bandwidth of 1 $cm^{-1}$.

## III. RESULTS

The ZEKE photoelectron spectra of the (1-0) and (0-0) bands of the $N_2^+X\,^2\Sigma_g^+ \leftarrow N_2X\,^1\Sigma_g^+$ transition are displayed in Figs. 1(a) and 1(b), respectively. It is immediately noticeable that the rotational structures of the

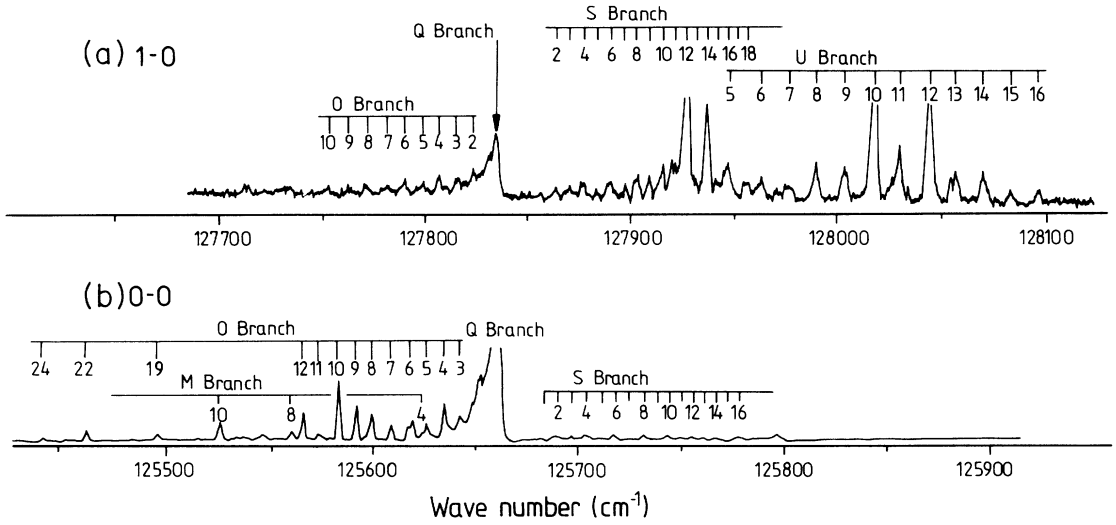


FIG. 1. ZEKE photoelectron spectra of nitrogen recorded with an extraction field of 1 V/cm, applied 500 ns after the laser pulse. (a) $N_2^+X\,^2\Sigma_g^+(v^+=1)\leftarrow N_2X\,^1\Sigma_g^+(v=0)$ band. (b) $N_2^+X\,^2\Sigma_g^+(v^+=0)\leftarrow N_2X\,^1\Sigma_g^+(v=0)$ band. The branch labels $M$, $O$, $Q$, $S$, and $U$ refer to the difference $(N^+-J'')$ between the rotational quantum number $N^+$ of the ion and the total-angular-momentum quantum number $J''$ of the neutral, with $(N^+-J'')$ equal to $-4$, $-2$, 0, $+2$, and $+4$, respectively.

two spectra are substantially different. The (0-0) band shows strong $O$ and $Q$ branches and a few $M$-branch lines [with $(N^+-J'')=-4$], but the $S$-branch intensity is very weak and no $U$ lines are seen. The (1-0) band is dominated by strong $S$ and $U$ branches, while the $Q$ and $O$ branches appear weaker and no $M$-branch lines are observed.

The large differences in branch intensities and propen-

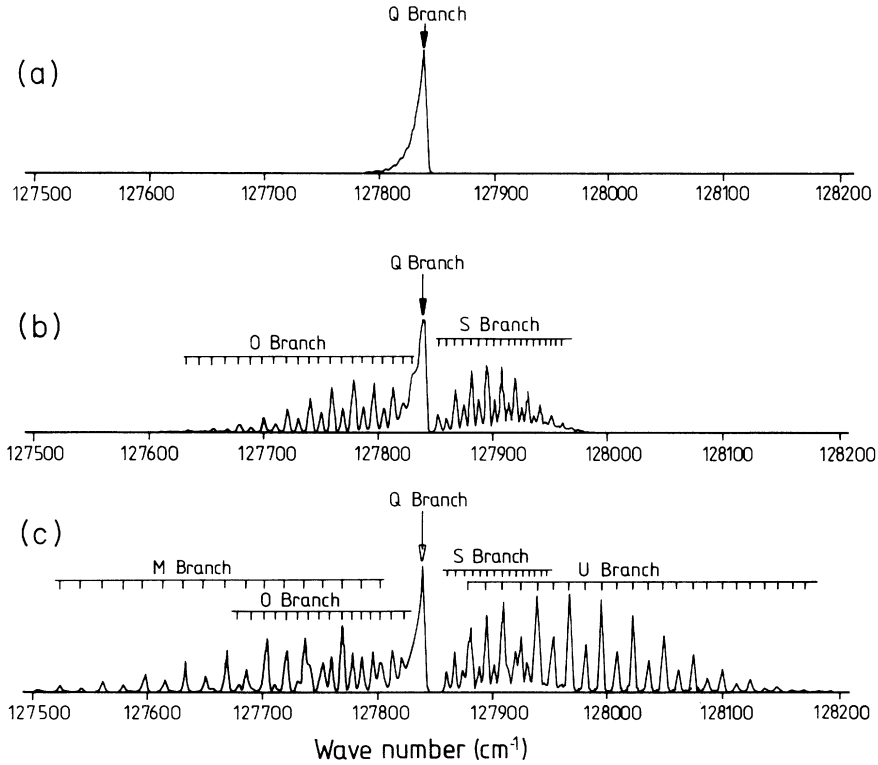


FIG. 2. Rotationally resolved ZEKE photoelectron spectra predicted for the $N_2^+X\,^2\Sigma_g^+\leftarrow N_2X\,^1\Sigma_g^+$ transition using the model of Buckingham, Orr, and Sichel [2]. (a)–(c) The $3\sigma_g$ orbital from which the electron is ejected is assumed to be a pure $s$, $d$, and $g$ single-center orbital, respectively. The lines are labeled as in Fig. 1.

sity rules existing between the two spectra cannot be explained by theoretical models like those proposed in Refs. [2] and [4], which are based on the expansion of the molecular valence orbital from which the electron is ejected. Indeed, in both cases, the electron is ejected from the same $3\sigma_g$ orbital of $N_2$, and therefore the two spectra in Fig. 1 should show similar intensity profiles. Figures 2(a)–2(c) show the contributions to the spectrum at room temperature predicted by using the theoretical model developed in Ref. [2] if one assumes that the $3\sigma_g$ molecular orbital can be represented by a pure *s*, *d*, and *g* single-center orbital, respectively. Clearly if the *S* or the *U* branches are strong, then one ought also to observe *O* and *M* branches and vice versa, in clear contradiction with the experiments (see Fig. 1). Furthermore, the simulations fail to account for the details of the rotational intensities within a given branch; in particular several *O* lines of the (0-0) band are missing or have a much weaker intensity than neighboring lines, like for instance *O*(11), *O*(13), *O*(14), *O*(15), *O*(16), *O*(17), *O*(18), *O*(20), *O*(21), and *O*(23); the *M* branch of the (0-0) band consists only of a few isolated lines [e.g., *M*(4), *M*(8) and *M*(10)] and does not show a regular progression; some lines of the (0-0) band have an asymmetric shape or appear as doublets [like *O*(6)]; finally the *S*(12), *S*(14), *U*(10), and *U*(12) lines of the (1-0) band have particularly large intensities compared to other *U*- and *S*-branch lines.

To properly account for all the observations one must remember that on the basis of conventional PES studies, it would be predicted that both the (0-0) and the (1-0) spectra should consist of a strong *Q* branch and weaker *O* and *S* branches [25,26]. It will be shown in Sec. IV how these observations can be explained by final-state interactions (or channel interactions).

## IV. DISCUSSION

### A. Intensity distortions of the 0-0 band: The effect of rotational autoionization

The Rydberg spectra of $N_2$ are dominated by *p* series [32,33] and weaker *f* series [34]. The transition intensity to high-lying *p* Rydberg states, belonging to series converging to the ground electronic state of the $N_2^+$ ion, is predominantly concentrated in the *Q* branch [33] (where again *Q* implies $N^+ - J'' = 0$). Since the electron signal detected in ZEKE studies stems from field ionization from high-Rydberg states, one expects to obtain ZEKE spectra consisting of a strong *Q* and weaker *O* and *S* branches.

As mentioned in Sec. III, the *O* branch of the ZEKE spectrum of the 0-0 band is as strong as the *Q* branch and one order of magnitude more intense than the *S* branch, in contrast to conventional PES results and the simulations in Fig. 2. This, and the somewhat unexpected intensity patterns listed in Sec. III, can be explained by the rotational autoionization mechanism illustrated in Fig. 3. As discussed above, the transitions to the Rydberg states lying just below the $J''-2, J''-4, J''-6, \ldots$ thresholds (which lead to *O*-, *M*-, *K*-, . . . branch ZEKE intensities) are weak, whereas transitions to Rydberg states converging to $N^+ = J''$ thresholds are strong. However, *O*-, *M*-, and *K*-branch ZEKE transitions can borrow intensity from the strong *Q* transitions to Rydberg states that converge to the $N^+ = J''$ limits and at the same time lie within the field ionization range of the *O*, *M*, and *K* limits, respectively. For example, the $n = 34$ and $n = 35$ Rydberg states converging to the $N^+ = 12$ limit are mixed, by the mechanism discussed below, with the pseudocontinuum of high-Rydberg states converging to the $N^+ = 10$ limit. Consequently, when the field is applied, these states can undergo rotational autoionization, and the *O*(12) ZEKE line apparently borrows intensity from the *Q*-branch transitions. Similarly, *M*(12) could borrow intensity from a transition to the $n = 26$ Rydberg state of the same series, as depicted in Fig. 3. It is important to note that rotational autoionization cannot lead to the enhancement of *S*-, or *U*-line intensities as the final ZEKE states are then degenerate with the continuum of the $N^+ = J''$ series. Indeed the interaction with the continuum could decrease the ZEKE intensities, as a result of rotational autoionization of the $N^+ = J'' + 2$, $N^+ = J'' + 4, \ldots$ states before the extraction field is applied.

Several models have been put forward to account for

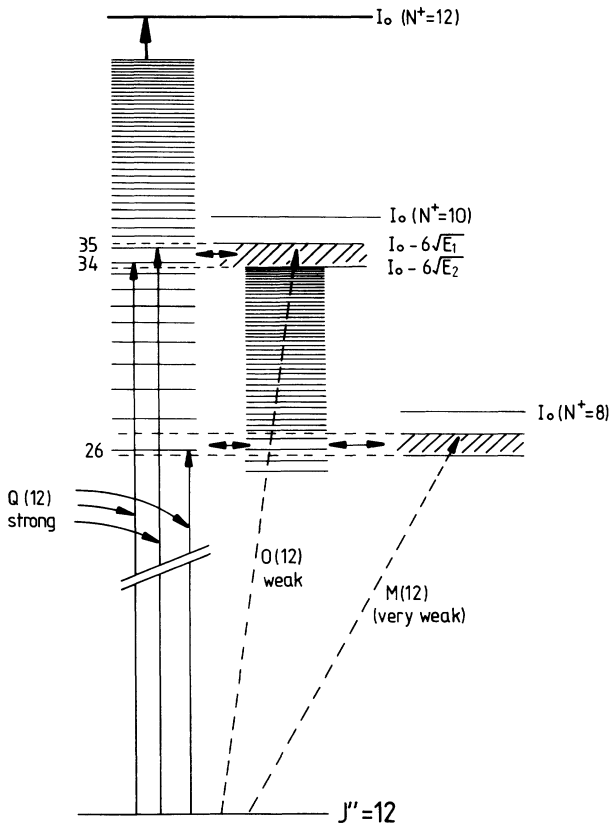


FIG. 3. Rotational autoionization mechanism explaining how weak *O* and *M* ZEKE transitions can borrow intensity from the strong *Q* transitions to Rydberg states converging on other limits. The mechanism involves a *j* step quadrupolar coupling between low- ($n = 20$–$60$) Rydberg states converging to the ($N^+ = J''$) rotational levels of the ion and high-Rydberg states ($n \gg 60$) converging to ($N^+ = J'' - 2j$) rotational levels of the ion.

the nature of the interaction that leads to rotational autoionization. In the absence of electric fields, rotational autoionization is caused by a coupling between core rotation and the Rydberg electron mediated by the dipole [17], the quadrupole or higher multipoles of the core [35]. The lowest nonvanishing multipole in $N_2$ is the quadrupole. Autoionization processes involving large changes $\Delta N^+$ in the rotational quantum number $N^+$ of the core have been discussed in detail by Mahon, Janik, and Gallagher [36] for $Li_2$. In the absence of electric fields, large $\Delta N^+$ can be caused either by direct multipole processes

$$(N^+,n,l)\rightarrow(N^+-2j,n_j,l+2j),\quad j=\text{positive integer} \tag{3}$$

or by a $j$-step quadrupole coupling enhanced by near-resonant intermediate states

$$\begin{aligned}(N^+,n,l)&\rightarrow(N^+-2,n_1,l_1)\\&\rightarrow(N^+-4,n_2,l_2)\\&\rightarrow\cdots\rightarrow(N^+-2j,n_j,l_j)\ ,\end{aligned} \tag{4}$$

where $n$ stands for the Rydberg quantum number and $l$ for the orbital angular-momentum quantum number of the Rydberg electron. The time scale of the former process is generally much slower than the time scale of the latter, especially when there is a large density of near-resonant states in the $j$-step process.

The quadrupole steps in Eq. (4) do not change the final-state total-angular momentum $J'$ ($J'=J_1=J_2=J_3$ in Fig. 4), but involve changes in $l$ of 0, $\pm2$. The quadrupole matrix elements involving $\Delta l=\pm2$ are about two orders of magnitude weaker than those involving $\Delta l=0$ [36]. In the case of $N_2$, where a $3\sigma_g$ electron is excited to

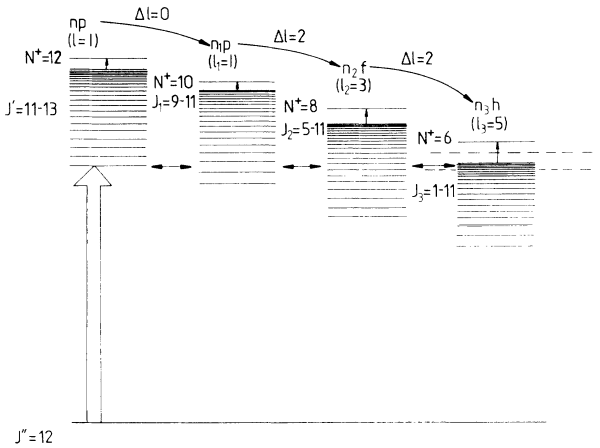


FIG. 4. Rotational autoionization process leading to large $\Delta N^+$ changes. The total-angular-momentum quantum numbers of the interacting channels are labeled $J'$, $J_1$, $J_2$, and $J_3$, respectively. If the autoionizing state is a $p$ Rydberg state and $J'=N^+-1$, then only one quadrupole step can involve a $\Delta l=0$ quadrupole matrix element. (This is so because the total angular momentum must be conserved.) The remaining steps must change the value of $l$ by $+2$.

a $np$ Rydberg orbital (with $l=1$), only one quadrupole step can be a $\Delta l=0$ process if $J'=N^+-1$, as illustrated in Fig. 4. For $J'=N^+$ or $N^++1$, no $\Delta l=0$ processes are possible. This is so because the total angular momentum $J'$ must be conserved throughout. If the electron were excited to an $nf$ Rydberg orbital, then two quadrupole steps could be $\Delta l=0$ processes for $J'=N^+-3$.

Whether the channel interaction with a given $\Delta N^+$ value takes place within a certain time (relevant in ZEKE spectroscopy is the time between the laser pulse and the application of the extraction voltage) depends on the number of quadrupole steps involved and the details of the near-resonant pathway. An estimate of the matrix elements involved appears to rule out, in the case of $Li_2$, any process with more than one $\Delta l=2$ step [36]. As a consequence, it is likely that changes of $\Delta N^+$ of up to $-4$ can be observed in ZEKE experiments on $N_2$ in the absence of electric fields for $J'=N^+-1$ states.

The situation is somewhat different in the presence of the stray electric field, as $l$ and $J'$ are no longer good quantum numbers. Instead of going through near-resonant pure-$l$ states, the enhancement pathway goes through Stark states that are a linear combination of pure-$l$ states. Under these circumstances, the complete many-step pathway can be formulated in terms of $\Delta l=0$ matrix elements [36]. Hence, in the presence of a field, transitions with large $\Delta N^+$ become observable in ZEKE experiments.

There are, however, two important restrictions to the maximum $\Delta N^+$ value that can be observed in a ZEKE spectrum by a field-induced rotational autoionization mechanism. First, Stark mixing by an electric field becomes less efficient at low $n$ values. Second, the number of autoionizing Rydberg states falling within the field-ionization range [defined by Eq. (1) or (2)] quickly decreases as $\Delta N^+$ becomes more negative and/or as the core rotational quantum numbers of the states involved increase, as can be seen from Figs. 3 and 4 and Table II.

To clearly establish that the enhanced intensity of the $O$ branch observed in the ZEKE spectrum of $N_2$ comes from the final-state interaction with higher-$N^+$, lower-$n$ Rydberg states, we have recorded a series of ZEKE spectra over a wide range of extraction voltages. Figures 5(a)–5(c) show the spectra recorded with one single extraction electric field of 16, 6, and 1 V/cm respectively, applied 500 ns after the laser pulse. The 1 V/cm spectrum is identical to the spectrum in Fig. 1(b). As the voltage is increased, more and more lines are observed, because the field ionization range is enlarged. As a result, the structure of the spectra becomes less and less ZEKE-like. The appearance of the spectrum resembles somewhat the $(1+1)$ ionization spectrum near the $X\,^2\Sigma_g^+(v^+=0,1)$ thresholds obtained by Trickl *et al.* [29]. The lines observed in both studies correspond to transitions to high-Rydberg states converging to some rotationally excited levels of the ion. The main differences are that in the $(1+1)$ resonance-enhanced multiphoton ionization study, the number of $N^+$ states observed is restricted by the selection of a specific rovibronic level in the first excitation step and that the symmetry of the intermediate resonant level imposes different selection rules

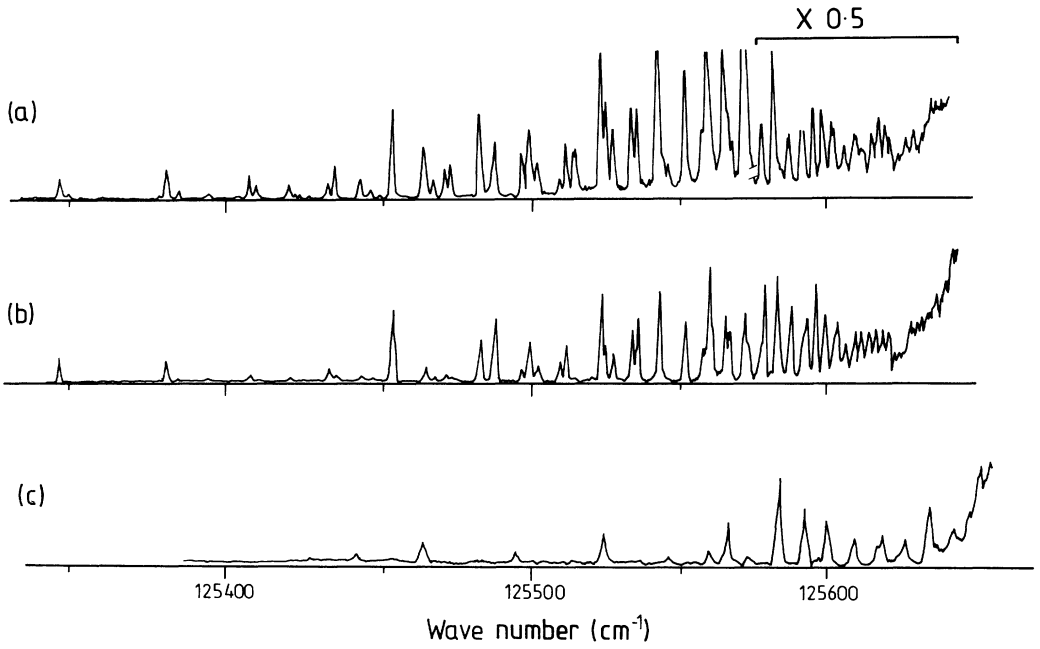


FIG. 5. ZEKE photoelectron-rotational autoionization spectra recorded with different extraction electric fields applied 500 ns after the laser pulse. The extraction fields corresponding to (a)–(c) are 16, 6, and 1 V/cm, respectively.

for ionization. Berkowitz and Ruscic have recorded a direct (one-photon) photoionization spectrum of $N_2$ near threshold and observed some undulations in the ionization cross section below the $v^+=0$ threshold [37]. These undulations were discussed in terms of field-induced autoionization of high-Rydberg states. However, the resolution of 6 $cm^{-1}$ in Ref. [37], combined with the fact that electrons released above threshold could not be discriminated against, prevented the authors from resolving any rotational structure. At high resolution and with the additional discrimination due to the pulsed extraction field, the undulations observed in Ref. [37] become the series of perfectly resolved and sharp lines seen in Fig. 5. All the lines observed in the spectra in Fig. 5 correspond to transitions to Rydberg states converging to $N^+=J''$ levels of the ion (i.e., $Q$-branch transitions) and can be unambiguously assigned using the standard Rydberg formula with a constant quantum defect $\delta$, and the known rotational constants for the ground state of the molecule $(B'',D'')$ and of the ion $(B^+,D^+)$:

$$\tilde{\nu}=\mathrm{IP}-\frac{R}{(n-\delta)^2}-\{(B''-B^+)J''(J''+1)-(D''-D^+)[J''(J''+1)]^2\}\ . \quad (5)$$

In Eq. (5) $R$ is the mass-corrected Rydberg constant for $N_2$. A total of 34 nonoverlapping lines with $n$ values between 20 and 40 were used to calculate the adiabatic ionization potential (IP) and the quantum defect $\delta$ in a least-squares-fit procedure. The experimental and calculated line positions are listed with assignment in Table I. The standard deviation of the fit is 0.19 $cm^{-1}$. Given the linewidth (1 $cm^{-1}$ full width at half maximum) of our XUV laser the agreement is excellent. Values of 125 668±0.25 $cm^{-1}$ and 0.641±0.016 $cm^{-1}$ are found for the ionization potential and quantum defect in Hund's case $d$, respectively. The error limits correspond to three standard deviations but do not account for a possible systematic error due to a slight displacement of $2\tilde{\nu}_1$ from exact two-photon resonance in Kr. These values are to be compared with the ionization potential of 125 667.032±0.2 $cm^{-1}$ and the Hund's-case-$b$ quantum defects $\mu_\sigma=0.608\,22\pm0.000\,48$ $cm^{-1}$ and $\mu_\pi=0.683\,75\pm0.000\,66$ $cm^{-1}$ determined by Huber and Jungen [32]. (For high values of the rotational quantum number of the ion, the Hund's-case-$d$ quantum defect is the average of the Hund's-case-$b$ quantum defects, i.e., 0.646 $cm^{-1}$, in good agreement with our result.)

A careful investigation of the influence of the magnitude of the electric field on the appearance of the spectra is of considerable help in assigning its rather complicated and irregular structure. It also leads to the determination of the final ionic state and the autoionization selection rule for each of the lines observed: If, for instance, a new line is observed at the wave number $\tilde{\nu}$ as the extraction voltage is increased from 2 to 3 V/cm, it *must* correspond to a transition to a Rydberg state lying between $6\sqrt{2}$ and $6\sqrt{3}$ $cm^{-1}$ below one of the $O$-, $M$-, $K$-, . . . ionization thresholds [see Eq. (1)]. This information, combined with the line position, is sufficient in most cases to unambiguously identify the threshold $(O,M,K,\ldots)$ in the field ionization range of which the Rydberg state has autoionized.

Once this information is obtained, it is trivial to determine the final ionic state, assuming that there is no further change of core rotation as the electron departs.

Figure 6 shows a comparison between the 6 V/cm spectrum [Fig. 6(b)] and a simulation [Fig. 6(a)] based on the following assumptions.

(1) The field-ionization range is taken from Eq. (2) with values of 6 and 0.09 V/cm for $E_2$ and $E_1$, respectively, corresponding to the values of the extraction and the stray electric field. This value for the stray field has not been measured but gives the best simulation of the experimental results.

(2) The $Q$ Rydberg states falling in the field ionization range corresponding to the $O$, $M$, and $K$ thresholds are assumed to autoionize with a probability of 1, 0.25, and 0.1, respectively, to take into account the fact that the time scale of the channel interaction increases with increasing $\Delta N^+$ value. These relative probabilities again give the best match to the experimental results.

(3) The intensity of the lines are weighted by appropriate population and spin statistics factors and by a $n^{-3}$ factor to take into account the dependence of the transition intensity on the quantum number $n$.

(4) The detection probability within the field ionization range is assumed to be constant and the effect of near-resonant pathways on line intensities is neglected.

The lines in Fig. 6 are labeled with the letters $O$, $M$, and $K$ corresponding to autoionization processes involving $\Delta N^+$ values of $-2$, $-4$, and $-6$, respectively. The additional label $N^+/n$ indicates the core rotational angular momentum $N^+$ and the Rydberg principal quantum number $n$. Given the crudeness of the assumptions made, the agreement is excellent: All the predicted $\Delta N^+ = -2$ and $\Delta N^+ = -4$ autoionization lines appear in the experimental spectrum. Furthermore experimental line intensities are well reproduced by the simulation. The agreement between predicted and experimental $\Delta N^+ = -6$ autoionization lines is by far not so good. In fact, apart from line $K$ 8/29, which has a similar intensity in the experimental and the simulated spectra, all other

TABLE I. Results of a least-squares fit of the experimental data (see Fig. 5) to Eq. (5) in the text. $N^+$ and $n$ are the upper-state quantum numbers. The only parameters fitted are the adiabatic ionization potential and the quantum defect. The standard deviation of the fit is 0.19 $cm^{-1}$.

| No. | $N^+$ | $n$ | $\tilde{\nu}_{expt}$ ($cm^{-1}$) | $\tilde{\nu}_{calc}$ ($cm^{-1}$) | $(\tilde{\nu}_{calc}-\tilde{\nu}_{expt})$ ($cm^{-1}$) |
|---|---|---|---|---|---|
| 1 | 20 | 20 | 125 347.28 | 125 347.20 | $-0.788\times10^{-1}$ |
| 2 | 18 | 21 | 125 380.34 | 125 380.52 | 0.182 |
| 3 | 28 | 23 | 125 394.10 | 125 393.98 | −0.112 |
| 4 | 17 | 22 | 125 407.14 | 125 407.16 | $0.210\times10^{-1}$ |
| 5 | 26 | 24 | 125 420.05 | 125 419.83 | −0.219 |
| 6 | 25 | 24 | 125 423.67 | 125 423.35 | −0.319 |
| 7 | 15 | 23 | 125 432.49 | 125 432.64 | 0.155 |
| 8 | 24 | 25 | 125 442.62 | 125 442.90 | 0.286 |
| 9 | 23 | 25 | 125 446.29 | 125 446.15 | −0.138 |
| 10 | 14 | 24 | 125 453.30 | 125 453.05 | −0.241 |
| 11 | 22 | 26 | 125 463.72 | 125 463.55 | −0.161 |
| 12 | 21 | 26 | 125 466.50 | 125 466.53 | $0.311\times10^{-1}$ |
| 13 | 13 | 25 | 125 470.70 | 125 471.11 | 0.417 |
| 14 | 20 | 27 | 125 481.99 | 125 482.06 | $0.790\times10^{-1}$ |
| 15 | 12 | 26 | 125 487.03 | 125 487.16 | 0.136 |
| 16 | 19 | 28 | 125 496.17 | 125 496.10 | $-0.663\times10^{-1}$ |
| 17 | 18 | 28 | 125 498.64 | 125 498.66 | $0.275\times10^{-1}$ |
| 18 | 11 | 27 | 125 501.49 | 125 501.48 | $-0.578\times10^{-2}$ |
| 19 | 9 | 27 | 125 504.66 | 125 504.31 | −0.349 |
| 20 | 18 | 29 | 125 508.91 | 125 508.82 | $-0.855\times10^{-1}$ |
| 21 | 17 | 29 | 125 511.15 | 125 511.25 | 0.102 |
| 22 | 16 | 30 | 125 522.85 | 125 522.68 | −0.168 |
| 23 | 10 | 29 | 125 524.31 | 125 524.45 | 0.146 |
| 24 | 8 | 29 | 125 526.97 | 125 527.01 | $0.434\times10^{-1}$ |
| 25 | 15 | 31 | 125 533.16 | 125 533.08 | $-0.726\times10^{-1}$ |
| 26 | 9 | 30 | 125 535.10 | 125 534.93 | −0.160 |
| 27 | 14 | 32 | 125 542.24 | 125 542.58 | 0.341 |
| 28 | 12 | 35 | 125 564.95 | 125 564.85 | $-0.962\times10^{-1}$ |
| 29 | 11 | 35 | 125 566.27 | 125 566.47 | 0.199 |
| 30 | 19 | 20 | 125 349.73 | 125 349.90 | 0.171 |
| 31 | 16 | 22 | 125 409.60 | 125 409.45 | −0.146 |
| 32 | 24 | 24 | 125 426.46 | 125 426.73 | 0.272 |
| 33 | 22 | 25 | 125 449.58 | 125 449.26 | −0.319 |
| 34 | 19 | 27 | 125 484.64 | 125 484.76 | 0.128 |

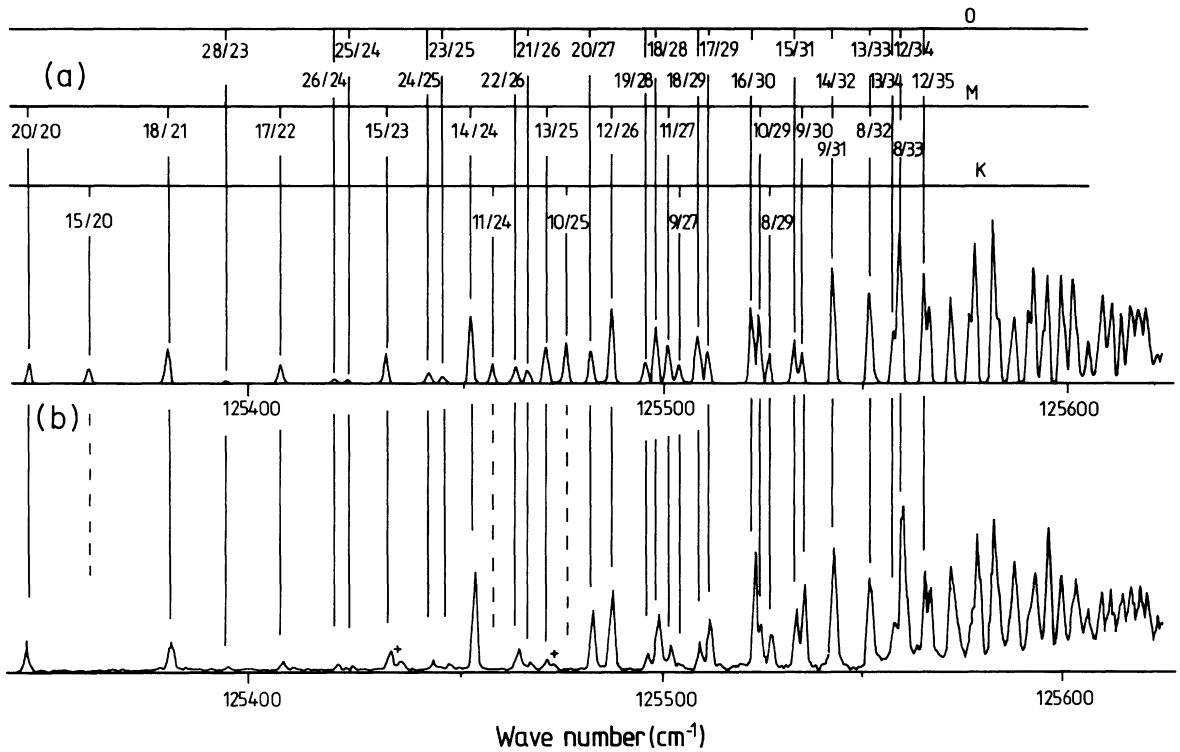


FIG. 6. Simulated (a) and experimental (b) ZEKE-rotational autoionization spectra of $N_2$ near the $X\,^2\Sigma_g^+(v^+=0)$ threshold corresponding to an extraction field of 6 V/cm. The assumptions made for the simulation are listed in the text. The lines correspond to transitions to Rydberg states converging to rotational levels of the ion with $N^+=J''$. They are labeled with $N^+/n$, where $N^+=J''$ is the rotational angular momentum of the ion core and $n$ is the Rydberg principal quantum number. A further label $O$, $M$, or $K$ indicates that the autoionization process involves changes in the rotational quantum number of the ion core of $-2$, $-4$, and $-6$, respectively.

$\Delta N^+=-6$ lines either appear much weaker ($K$ 9/27) or are completely missing ($K$ 15/20, $K$ 11/24, $K$ 10/25). Only two weak lines marked with a "+" in Fig. 6(b) remain unassigned. They cannot be accounted for by any rotational autoionization mechanism involving $\Delta N^+$ changes up to $-8$.

These propensity rules can be understood as follows: As discussed above, autoionization processes with $\Delta N^+=-2$ and $\Delta N^+=-4$ should be sufficiently fast to be observed in the absence of an electric field, at least for $J'=N^+-1$ (see Fig. 4). On the other hand, autoionization processes with $\Delta N^+=-6$ should not be observed unless the near-resonant pathway is particularly efficient, as they require two $\Delta l=+2$ steps in Eq. (4).

To investigate the effect of near-resonant pathways in more detail, we calculated the frequencies of all possible Rydberg states involved in the various steps of Eq. (4) for each of the $\Delta N^+=-6$ processes predicted in the 6 V/cm spectrum. The results are summarized in Table II: A $\Delta N^+=-6$ process involves three quadrupole steps (see Figs. 3 and 4). The first one is between Rydberg states converging to $N^+=J''$ limits with $n$ values between 14 and 37 and Rydberg states converging to $N^+=J''-2$ limits with $n$ values between 17 and 48. The second step couples these latter Rydberg states and Rydberg states converging to $N^+=J''-4$ limits with $n$ values between 27 and 72. The last quadrupole step causes an interaction between these and the very-high-Rydberg states (with $n\geq 85$) lying in the field-ionization range of the $N^+=J''-6$ limits. Since the density of Rydberg states per $cm^{-1}$ is proportional to $n^3$, some of the Rydberg states involved in the third quadrupole step are very likely to be nearly degenerate and hence the condition for an efficient near-resonant pathway is fulfilled to a good approximation. This near-resonance condition is likely to be met reasonably well in the second quadrupole step too, especially for processes involving low-$J''$ values (see Table II). At higher-$J''$ values, near resonances in the second step become less and less frequent and, as a result, the corresponding $\Delta N^+=-6$ lines are not observed experimentally. The first quadrupole step involves the lowest-Rydberg states and is the least likely to couple near-resonant Rydberg states. It can be seen in Table II that the near-resonance condition in the first quadrupole step is best met for line $K$ 8/29, which happens to be the only strong line autoionizing with $\Delta N^+=-6$ to be observed in the experimental spectrum (see Fig. 6). It should be noted that for molecules with smaller rotational constants than those of $N_2$, autoionization processes involving more quadrupole steps (and hence leading to larger $\Delta N^+$ changes) should be observable, because, for

TABLE II. Near resonant autoionization pathways for the lines that are predicted to autoionize with $\Delta N^+ = -6$, for an extraction field of 6 V/cm. The autoionization mechanism is illustrated in Figs. 3 and 4 and described in detail in the text. All the wave numbers have been calculated using Eq. (5).

| $Q$ Rydberg transitions lying in the field-ionization range of $K$ thresholds | | | | Near-resonant $O$ Rydberg transitions | | | Near-resonant $M$ Rydberg transitions | | | Near-resonant $K$ Rydberg transitions | | |
|---|---|---|---|---|---|---|---|---|---|---|---|---|
| $J''$ | $N^+$ | $n$ | $\tilde{\nu}$ (cm$^{-1}$) | $N^+$ | $n$ | $\tilde{\nu}$ (cm$^{-1}$) | $N^+$ | $n$ | $\tilde{\nu}$ (cm$^{-1}$) | $N^+$ | $n$ | $\tilde{\nu}$ (cm$^{-1}$) |
| 6 | 6 | 35 | 125 572.52 | 4 | 47 | 125 572.13 | 2 | 68 | 125 572.10 | 0 | 85 | 125 569.31 |
| | | | | 4 | 48 | 125 574.27 | 2 | 69 | 125 572.80 | | | |
| | | | | | | | 2 | 70 | 125 573.47 | | to | |
| | | | | | | | 2 | 71 | 125 574.11 | | | |
| | | | | | | | 2 | 72 | 125 574.73 | 0 | 240 | 125 582.81 |
| 6 | 6 | 36 | 125 577.71 | 4 | 49 | 125 576.27 | 2 | 74 | 125 575.89 | 0 | 85 | 125 569.31 |
| | | | | 4 | 50 | 125 578.15 | 2 | 75 | 125 576.44 | | | |
| | | | | | | | 2 | 76 | 125 576.96 | | to | |
| | | | | | | | 2 | 77 | 125 577.46 | | | |
| | | | | | | | 2 | 78 | 125 577.94 | | | |
| | | | | | | | 2 | 79 | 125 578.40 | 0 | 240 | 125 582.81 |
| 6 | 6 | 37 | 125 582.47 | 4 | 52 | 125 581.59 | 2 | 87 | 125 581.57 | 0 | 85 | 125 569.31 |
| | | | | 4 | 53 | 125 583.16 | 2 | 88 | 125 581.90 | | | |
| | | | | | | | 2 | 89 | 125 582.23 | | to | |
| | | | | | | | 2 | 90 | 125 582.54 | | | |
| | | | | | | | 2 | 91 | 125 582.84 | | | |
| | | | | | | | 2 | 92 | 125 583.13 | | | |
| | | | | | | | 2 | 93 | 125 583.42 | 0 | 240 | 125 582.81 |
| 7 | 7 | 32 | 125 552.95 | 5 | 42 | 125 550.42 | 3 | 61 | 125 549.85 | 1 | 85 | 125 545.31 |
| | | | | 5 | 43 | 125 553.41 | 3 | 62 | 125 550.82 | | | |
| | | | | | | | 3 | 63 | 125 551.75 | | to | |
| | | | | | | | 3 | 64 | 125 552.63 | | | |
| | | | | | | | 3 | 65 | 125 553.47 | 1 | 240 | 125 558.81 |
| 8 | 8 | 29 | 125 527.01 | 6 | 37 | 125 522.80 | 4 | 52 | 125 521.92 | 2 | 85 | 125 521.19 |
| | | | | 6 | 38 | 125 527.18 | 4 | 53 | 125 523.50 | | | |
| | | | | | | | 4 | 54 | 125 524.98 | | to | |
| | | | | | | | 4 | 55 | 125 526.39 | | | |
| | | | | | | | 4 | 56 | 125 527.72 | 2 | 240 | 125 534.69 |
| 9 | 9 | 27 | 125 504.31 | 7 | 35 | 125 503.96 | 5 | 51 | 125 503.68 | 3 | 85 | 125 496.88 |
| | | | | 7 | 36 | 125 509.15 | 5 | 52 | 125 505.35 | | | |
| | | | | | | | 5 | 53 | 125 506.92 | | to | |
| | | | | | | | 5 | 54 | 125 508.41 | | | |
| | | | | | | | 5 | 55 | 125 509.81 | 3 | 240 | 125 510.37 |
| 10 | 10 | 25 | 125 475.96 | 8 | 31 | 125 468.83 | 6 | 42 | 125 466.09 | 4 | 85 | 125 472.50 |
| | | | | 8 | 32 | 125 476.30 | 6 | 43 | 125 469.09 | | | |
| | | | | | | | 6 | 44 | 125 471.87 | | to | |
| | | | | | | | 6 | 45 | 125 474.48 | | | |
| | | | | | | | 6 | 46 | 125 476.91 | 4 | 240 | 125 486.0 |
| 11 | 11 | 24 | 125 458.31 | 9 | 30 | 125 451.43 | 7 | 42 | 125 449.26 | 5 | 85 | 125 448.00 |
| | | | | 9 | 31 | 125 459.68 | 7 | 43 | 125 452.25 | | | |
| | | | | | | | 7 | 44 | 125 455.04 | | to | |
| | | | | | | | 7 | 45 | 125 457.64 | | | |
| | | | | | | | 7 | 46 | 125 460.07 | 5 | 240 | 125 461.50 |
| 15 | 15 | 20 | 125 359.34 | 13 | 25 | 125 355.86 | 11 | 35 | 125 351.82 | 9 | 85 | 125 348.62 |
| | | | | 13 | 26 | 125 370.15 | 11 | 36 | 125 357.00 | | | |
| | | | | | | | 11 | 37 | 125 361.76 | | to | |
| | | | | | | | 11 | 38 | 125 366.15 | | | |
| | | | | | | | 11 | 39 | 125 370.20 | | | |
| | | | | | | | 11 | 40 | 125 373.94 | 9 | 240 | 125 362.13 |
| 16 | 16 | 19 | 125 324.42 | 14 | 23 | 125 311.48 | 12 | 31 | 125 308.23 | 10 | 85 | 125 323.50 |
| | | | | 14 | 24 | 125 329.87 | 12 | 32 | 125 315.71 | | | |
| | | | | | | | 12 | 33 | 125 322.50 | | to | |
| | | | | | | | 12 | 34 | 125 328.69 | | | |
| | | | | | | | 12 | 35 | 125 334.34 | 10 | 240 | 125 337.00 |

TABLE II. (*Continued*).

| $Q$ Rydberg transitions lying in the field-ionization range of $K$ thresholds | | | | Near-resonant $O$ Rydberg transitions | | | Near-resonant $M$ Rydberg transitions | | | Near-resonant $K$ Rydberg transitions | | |
|---|---|---|---|---|---|---|---|---|---|---|---|---|
| $J''$ | $N^+$ | $n$ | $\tilde{\nu}$ (cm$^{-1}$) | $N^+$ | $n$ | $\tilde{\nu}$ (cm$^{-1}$) | $N^+$ | $n$ | $\tilde{\nu}$ (cm$^{-1}$) | $N^+$ | $n$ | $\tilde{\nu}$ (cm$^{-1}$) |
| 18 | 18 | 18 | 125 281.11 | 16 | 22 | 125 270.43 | 14 | 30 | 125 264.65 | 12 | 85 | 125 272.81 |
| | | | | 16 | 23 | 125 291.46 | 14 | 31 | 125 272.90 | | | |
| | | | | | | | 14 | 32 | 125 280.37 | | to | |
| | | | | | | | 14 | 33 | 125 287.16 | | | |
| | | | | | | | 14 | 34 | 125 293.35 | 12 | 240 | 125 286.31 |
| 20 | 20 | 17 | 125 229.96 | 18 | 21 | 125 225.67 | 16 | 29 | 125 219.67 | 14 | 85 | 125 221.69 |
| | | | | 18 | 22 | 125 249.88 | 16 | 30 | 125 228.81 | | | |
| | | | | | | | 16 | 31 | 125 237.06 | | to | |
| | | | | | | | 16 | 32 | 125 244.53 | | | |
| | | | | | | | 16 | 33 | 125 251.32 | 14 | 240 | 125 235.19 |
| 29 | 29 | 14 | 124 994.66 | 27 | 17 | 124 981.49 | 25 | 23 | 124 969.17 | 23 | 85 | 124 985.56 |
| | | | | 27 | 18 | 125 027.37 | 25 | 24 | 124 987.74 | | | |
| | | | | | | | 25 | 25 | 125 003.73 | | to | |
| | | | | | | | 25 | 26 | 125 018.04 | | | |
| | | | | | | | 25 | 27 | 125 030.74 | 23 | 240 | 124 999.06 |

these molecules, the $O$, $M$, $K$, . . . thresholds lie closer together, and the density of Rydberg states coupled in a given quadrupole step is higher.

In the presence of an electric field (the stray field in our experiments), $\Delta N^+ = -2, -4, -6, \ldots$ autoionization rates can be enhanced significantly. In our spectra the effect of the stray field does not seem to be sufficient for autoionization processes involving $\Delta N^+$ changes greater in magnitude than $-4$ to be observed within 500 ns. However, it cannot be ruled out that the timescale of $\Delta N^+ = -2$ or $\Delta N^+ = -4$ autoionization processes is reduced by the presence of the stray field.

All the unexpected intensity patterns observed in the ZEKE spectrum [Fig. 1(b)] of the (0-0) band can be explained by rotational autoionization: Line $O(6)$ appears as a doublet because two Rydberg states (with $N^+ = 6$ and $n = 48, 49$) fall in the field-ionization range below the $N^+ = 4$ threshold. Some of the $O$- and $M$-branch lines are not observed (see Sec. III) because no Rydberg states converging to the $N^+ = J''$ thresholds lie within the corresponding $N^+ = J'' - 2$ and $N^+ = J'' - 4$ field-ionization ranges.

### B. Intensity distortions in the (1-0) band: The effect of a complex resonance

The ZEKE spectrum of the (1-0) band of $N_2$ [Fig. 1(a)] does not show particularly strong $O$- and $M$-line intensities but possesses very intense $S$ and $U$ branches. It was pointed out in Sec. IV A that, whereas a rotational autoionization mechanism can considerably enhance $O$- and $M$-branch intensities, it cannot account for unexpectedly strong $S$ and $U$ branches. The fact that lines $S(12)$ and $U(10)$ [and also $S(14)$ and $U(12)$] appear as the strongest in the spectrum and lead to the same final states seems to indicate a final-state interaction. The mechanism proposed involves a complex resonance.

Complex resonances are well known in the photoionization spectra of $H_2$ [38] and $N_2$ [39,40]. For $N_2$, Dehmer, Miller, and Chupka [39] have identified a series of complex resonances, one of them very close to the (1-0) ionization threshold (between 127 520 and 127 680 cm$^{-1}$). This complex resonance has been interpreted as a combined interaction between the continuum above the $v^+ = 0$ threshold with high-lying Rydberg states converging to the $v^+ = 1$ level of $N_2^+$ and two interloper states converging to the $A\,^2\Pi_u$ state, namely the $(v = 0, n = 4)5s\sigma g$ and the $(v = 3, n = 3)4s\sigma g$ Rydberg states [40]. The couplings are illustrated in the generalized picture of Fig. 7(a), where $A$ represents the interlop-

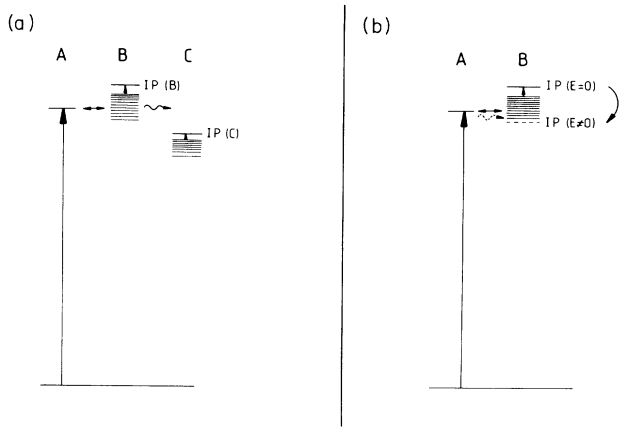


FIG. 7. (a) The interaction scheme typical for a complex resonance. Two closed channels ($A$ and $B$) interact with each other and are coupled to a third open channel $C$. In a pulsed electric field experiment channel $B$ can be converted into an open channel when the ionization threshold is lowered by the field, leading to a new autoionization pathway (b).

er states, $B$ the $v^+=1$ states, and $C$ the $v^+=0$ continuum. Another photoionization peak appears at slightly higher frequencies in the spectrum of Dehmer, Miller, and Chupka between 127 800 and 128 100 $cm^{-1}$ and still remains unassigned. This range of frequencies exactly corresponds to the region where the strong $S$ and $U$ ZEKE branches are observed [see Fig. 1(a)]. There is indeed a direct correspondence between the photoionization intensity and the ZEKE intensities as can be seen from Fig. 8. Figure 8(a) was recorded by measuring the electron production by applying an extraction field (3 V/cm) directly after the laser pulse. The line profile is similar to the photoionization peak observed by Dehmer, Miller, and Chupka [39]. The spectra in Figs. 8(b) and 8(c) were obtained by delaying the extraction field by 30 and 60 ns, respectively, and one can see clearly how the $Q$, $S$, and $U$ branches of the ZEKE spectrum gradually materialize out of the photoionization band to lead finally to the spectrum shown in Fig. 1(a). We propose that this interloper state forms a complex resonance with the high-$n$, $v^+=1$ Rydberg states and also the $v^+=0$ continuum, leading to the observed intensity perturbations in the ZEKE spectrum. However, in this case, the high-$n$, $v^+=1$ states are only very weakly coupled to the continuum, and the primary decay mechanism is to the $v^+=1$ channel.

The exact nature of the photoionization peak in Fig. 8(a) is not known. It is unlikely to be a member of one of the ns series converging the $A\,^2\Pi_u(v^+=0\rightarrow 7)$ states of $N_2^+$, as these states have all been assigned [39,41,43]. The components of the Rydberg series converging to the $B$ state of $N_2^+$ lie above 130 000 $cm^{-1}$ and can also be ruled out. We speculate that the interloper state is one of the $4d$ $v^+=0$ Rydberg states converging to the $A\,^2\Pi_u$ state of the ion, probably the $4d\delta_g$ state, as illustrated in Fig. 9. This is supported by the calculations of Duzy and Berry that suggest that $nd\delta_g$ Rydberg states have oscillator strengths that are comparable to those of the $ns\sigma_g$ states and that the transition frequency to the $4d\delta_g$ state lies near 128 000 $cm^{-1}$ [44]. An alternative possibility for the interloper state is the $v^+=2$ $3d\sigma_g$ Rydberg state [42]. Coupling of this interloper state with the continuum above the $v^+=1$ threshold leads to direct autoionization and ions with $v^+=1$ are formed. Coupling below the $v^+=1$ continuum does not lead to the formation of ions with $v^+=1$; however, autoionization to the $v^+=0$ threshold can occur, either directly, or indirectly through a complex resonance mechanism [as in Fig. 7(a)]. In the presence of an electric field, the $v^+=1$ limit is lowered and some states that lie below the field-free $v^+=1$ threshold can autoionize directly to the $v^+=1$ continuum [as in Fig. 7(b)].

An important question that arises concerns lifetimes: The photoionization peak around 128 000 $cm^{-1}$ in Ref. [39] and Fig. 8(a) is strong. This suggests an efficient and quick autoionization mechanism for the interloper state. But, if this is the case, why is it possible that the $U$- and $S$-branch ZEKE lines borrow intensity from a transition to this interloper state, given that the ZEKE extraction field is applied 500 ns after the excitation, and therefore only long-lived states are detected? The only answer to that question is that some states are not efficiently autoionized until the extraction field is turned on and lowers the $v^+=1$ limit. Autoionization to the $v^+=0$ continuum by the complex resonance mechanism [Fig. 7(a)] is not fast enough to completely quench the ZEKE signal within 500 ns.

From these considerations, one can conclude that the

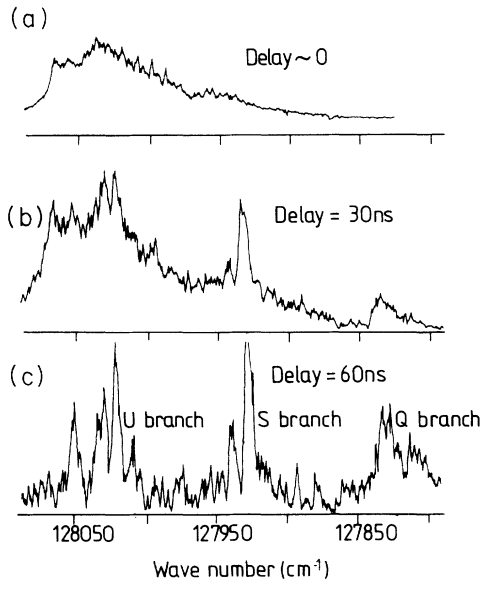


FIG. 8. Effect of the delay time before the application of the extraction voltage on the ZEKE photoelectron spectrum of the $N_2^+X\,^2\Sigma_g^+(v^+=1)\leftarrow N_2X\,^1\Sigma_g^+(v=0)$ transitions. A 3 V/cm extraction field was applied 0, 30, and 60 ns after the laser pulse leading to the spectra (a)–(c).

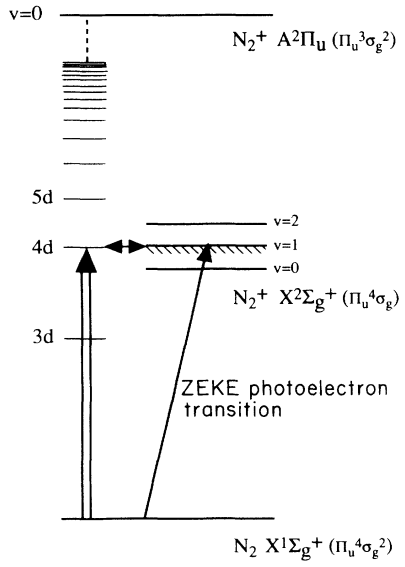


FIG. 9. Possible interpretation of the autoionization peak observed in Fig. 7(a). A $d$-Rydberg state (possibly the $4d\delta_g$ state) interacts strongly with the high-Rydberg states leading to the $X\,^2\Sigma_g^+(v^+=1)$ limit of $N_2^+$ and with the continuum above this limit. These two channels are weakly coupled to the $X\,^2\Sigma_g^+(v^+=0)$ continuum and form a complex resonance.

ZEKE signals in Fig. 8 come from field-induced electronic autoionization of that part of the complex resonance lying in the field-ionization range below one of the $v^+=1$ ionization thresholds. The situation is illustrated in Fig. 10; a complex resonance occurs between a particular rotational level of the interloper state and the continuum–high-Rydberg states converging on a particular rotational level of the ion with $v^+=1$. The result is the Lorentzian distribution of transition intensity shown at the right of the figure. However, only the shaded part of the resonances are observed in the ZEKE spectra.

This explains why the delayed-pulsed-field experiment leads to a rotationally resolved spectrum while the nondelayed or continuous-field experiment does not. In a pulsed-field experiment [Figs. 1(a), 8(b), and 8(c)], the electrons that are produced by direct autoionization above the $v^+=1$ thresholds before the extraction voltage is applied are removed from the ionization region by the small stray field present in our experiment and do not contribute to the ZEKE signal. The intensity of the various rotational components of the ZEKE spectrum is proportional to the integrated intensity of the complex resonance within the field-ionization range. In the continuous-field-photoionization spectrum of Dehmer, Miller, and Chupka [39], the entire Lorentzian profile is detected.

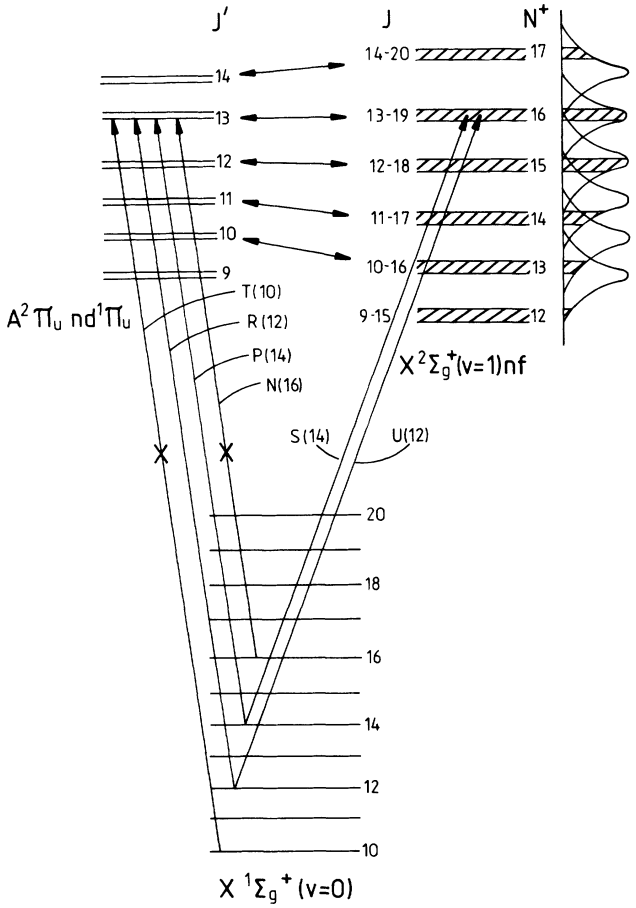


FIG. 10. Diagram illustrating how the *S*- and *U*-branch intensity of the (1-0) ZEKE band can be enhanced by final-state interaction while the *W*-, *Q*-, *O*-, and *M*-branch intensity cannot, assuming that the *P*- and *R*-branch transitions to the interloper state are the only branches with significant intensity. The ZEKE rotational-line intensities correspond to the integrated intensity of the complex resonance within the field ionization range shown at the far right. Details of labels are given in the text.

Figure 10 shows how an interloper ($A\,^2\Pi_u$) $nd\,^1\Pi_u$ Rydberg state could selectively enhance *S*- and *U*-branch intensities and not *Q*-, *O*-, *M*-, and *W*-branch intensities. The rotational levels of the interloper are assumed to behave as Hund's case *b* (even though the $4d\delta_g/3d\sigma_g$ states are probably intermediate between Hund's case *b* and *d*) and are labeled with the rotation quantum number $J'$. Each of these levels interacts with very-high-lying $nf$ Rydberg states converging to the $X\,^2\Sigma_g^+ v^+=1$ levels of the ion. These Rydberg states are described by Hund's case *d* and the possible $J$ values corresponding to a given $N^+$ value lie between $N^++3$ and $N^+-3$ (here spin is neglected). The interaction takes place at constant $J$ ($J'-J=0$). One can immediately see from Fig. 10 that if the only transitions to the interloper state were *P*, *Q*, and *R* lines, *U*(12) and *S*(14) could borrow intensity from a transition to the $J'=13$ interloper state, but *W*(10), *Q*(16), *O*(18), and *M*(20) would not, since the $J'=13$ interloper level $J'=13$ would have no transition intensity from ground-state levels with $J''=10$, 16, 18, or 20.

## V. CONCLUSION

The ZEKE photoelectron spectra of the $X\,^2\Sigma_g^+(v^+=0,1)\leftarrow X\,^1\Sigma_g^+(v=0)$ bands of nitrogen have been recorded at a resolution sufficient to observe the rotational structure. The two bands show very different intensity patterns and propensity rules for ionization. The (0-0) band consists of strong *Q* and *O* branches and weak *M* and *S* branches. The (1-0) band possesses very strong *S* and *U* branches in addition to the *Q* and *O* branches. The intensity patterns are discussed in terms of final-state (or channel) interactions. The intensity distortions in the (0-0) band are shown to be due to rotational autoionization. The interactions are induced by the ion-core quadrupole and may be assisted by the stray field. The autoionization only occurs when the ionization thresholds are lowered by the extraction field. Recording ZEKE spectra of the (0-0) band with large extraction voltages led to the recording of very nicely resolved rotational autoionization spectra of high-Rydberg states converging to the rotational levels of the $X\,^2\Sigma_g^+ v^+=0$ limit. All the observed transitions to Rydberg states are *Q*-branch lines (that is to say that the core angular-momentum number $N^+$ is equal to the angular-momentum quantum number $J''$ of the neutral). A careful investigation of the effect of the magnitude of the extraction electric field on the number and the position of the lines observed leads to the characterization of the final ionic state produced in the rotational autoionization process and consequently to the obtaining of propensity rules for autoionization. In $N_2$, rotational autoionization processes with $\Delta N^+=-2$ and $-4$ appear as strong lines whereas processes with

$\Delta N^+ = -6$ are much weaker. No autoionizing lines with $\Delta N^+ = -8$ are observed. These results are discussed within the model proposed by Mahon, Janik, and Gallagher [36] to account for the rotational selection rules observed in $Li_2$ in the presence of electric fields. For molecules with smaller rotational constants than $N_2$, we expect that autoionization processes involving larger changes in the rotational angular momentum of the core should be observed.

The unexpected intensity patterns in the (1-0) band are explained by a complex resonance mechanism. An interaction scheme is proposed that explains why the spectrum is composed of strong $S$ and $U$ branches while no $M$ branch is observed. The mechanism could be tested by multichannel quantum defect theory.

The ZEKE spectra of $N_2$ reported here are another example of the dramatic effect of final-state interactions on ZEKE rotational-line intensities. The mechanisms leading to intensity distortions are likely to be quite general and have been found to affect the ZEKE rotational intensity distributions in other systems [13–16]. It is clear that, although the prediction of ZEKE rotational-line intensities and selection rules based on theoretical models that neglect final-state interactions are still useful in some cases, one will in the future need to include these interactions in order to gain a complete picture of the mechanisms leading to ZEKE rotational-line intensities.

Finally, recording photoelectron spectra with pulsed delayed-extraction fields appears not only to be an attractive method to obtain rovibronic energy levels of ions but seems ideally suited to investigate interactions between very-high-Rydberg states.

## ACKNOWLEDGMENTS

We would like to thank Miss H. H. Fielding for her work in the setting up of the equipment and Dr. M. S. Child and Dr. R. S. Gilbert for helpful discussions. We are grateful to the Royal Society Paul Fund and the SERC for financial support and to Magdalene College Cambridge for additional support for one of us (F.M.).

[1] K. Müller-Dethlefs and E. W. Schlag, Ann. Rev. Phys. Chem. **42**, 109 (1991).
[2] A. D. Buckingham, B. J. Orr, and J. M. Sichel, Philos. Trans. R. Soc. London A **268**, 147 (1970).
[3] L. Åsbrink, Chem. Phys. Lett. **7**, 549 (1970).
[4] Y. Itikawa, Chem. Phys. **28**, 461 (1978).
[5] S. N. Dixit, D. L. Lynch, V. McKoy, and W. M. Huo, Phys. Rev. A **32**, 1267 (1985).
[6] J. Xie and R. N. Zare, J. Chem. Phys. **93**, 3033 (1990).
[7] K. Müller-Dethlefs, J. Chem. Phys. **95**, 4822 (1991).
[8] K. Wang, J. A. Stephens, and V. McKoy, J. Chem. Phys. **95**, 6456 (1991).
[9] R. G. Tonkyn, J. W. Winniczek, and M. G. White, Chem. Phys. Lett. **164**, 137 (1989).
[10] H. H. Fielding, T. P. Softley, and F. Merkt, Chem. Phys. **155**, 257 (1991).
[11] R. T. Wiedmann, E. R. Grant, R. G. Tonkyn, and M. G. White, J. Chem. Phys. **95**, 746 (1991).
[12] M. Braunstein, V. McKoy, S. N. Dixit, R. G. Tonkyn, and M. G. White, J. Chem. Phys. **93**, 5345 (1990).
[13] R. G. Tonkyn, R. Wiedmann, E. R. Grant, and M. G. White, J. Chem. Phys. **95**, 7033 (1991).
[14] F. Merkt and T. P. Softley, J. Chem. Phys. **96**, 4149 (1992).
[15] G. Reiser and K. Müller-Dethlefs, J. Phys. Chem. **96**, 9 (1992).
[16] E. Grant and M. G. White, Nature **354**, 249 (1991).
[17] R. Gilbert and M. S. Child, Chem. Phys. Lett. **187**, 153 (1991).
[18] T. Baer and B. P. Tsai, J. Electron Spectrosc. Relat. Phenom. **2**, 25 (1973).
[19] Wm. B. Peatman, B. Gotchev, P. Gürtler, E. E. Koch, and V. Saile, J. Chem. Phys. **69**, 2089 (1978).
[20] T. Baer and P. M. Guyon, J. Chem. Phys. **85**, 4765 (1986).
[21] G. Herzberg and Ch. Jungen, J. Mol. Spectrosc. **41**, 425 (1972).
[22] A. W. Potts and T. A. Williams, J. Electron Spectrosc. **3**, 3 (1974).
[23] J. Berkowitz and W. A. Chupka, J. Chem. Phys. **51**, 2341 (1969).
[24] A. Katrib, T. P. Debies, R. J. Colton, T. H. Lee, and J. W. Rabalais, Chem. Phys. Lett. **22**, 196 (1973).
[25] J. D. Allen and F. A. Grimm, Chem. Phys. Lett. **66**, 72 (1979).
[26] P. Baltzer, L. Karlsson, and B. Wannberg, Phys. Rev. A **46**, 315 (1992).
[27] M. A. Duncan, T. G. Dietz, and R. E. Smalley, J. Chem. Phys. **75**, 2118 (1981).
[28] K. H. Fung, H. L. Selzle, and E. W. Schlag, Z. Naturforsch. A **36**, 1257 (1981).
[29] T. Trickl, E. F. Cromwell, Y. T. Lee, and A. H. Kung, J. Chem. Phys. **91**, 6006 (1989).
[30] E. D. Poliakoff, J. L. Dehmer, A. C. Parr, and G. E. Leroi, Chem. Phys. Lett. **111**, 128 (1984).
[31] G. Reiser, W. Habenicht, K. Müller-Dethlefs, and E. W. Schlag, Chem. Phys. Lett. **152**, 119 (1988).
[32] K. P. Huber and Ch. Jungen, J. Chem. Phys. **92**, 850 (1990).
[33] P. K. Carroll and K. Yoshino, J. Phys. B **5**, 1614 (1972).
[34] F. S. Chang and K. Yoshino, J. Phys. B **16**, 6581 (1983).
[35] E. E. Eyler and F. M. Pipkin, Phys. Rev. A **27**, 2462 (1983).
[36] C. R. Mahon, G. R. Janik, and T. F. Gallagher, Phys. Rev. A **41**, 3746 (1990).
[37] J. Berkowitz and B. Ruscic, J. Chem. Phys. **93**, 1741 (1990).
[38] M. Raoult and Ch. Jungen, Faraday Discuss. Chem. Soc. **71**, 253 (1981).
[39] P. M. Dehmer, P. J. Miller, and W. A. Chupka, J. Chem. Phys. **80**, 1030 (1984).
[40] A. Giusti-Suzor and H. Lefebvre-Brion, Phys. Rev. A **30**, 3057 (1984).
[41] M. Ogawa and Y. Tanaka, Can. J. Phys. **40**, 1593 (1962).
[42] H. Lefebvre-Brion, private communication.
[43] K. Yoshino, M. Ogawa, and Y. Tanaka, J. Mol. Spectrosc. **61**, 403 (1976).
[44] C. Duzy and R. S. Berry, J. Chem. Phys. **64**, 2421 (1976).